PVP2007-26139

EFFICACY OF A SLIDING BEAM AS A NONLINEAR VIBRATION ISOLATOR

R. A. Ibrahim
Wayne State University
Department of Mechanical Engineering
Detroit, MI 48202

R. J. Somnay
Wayne State University
Department of Mechanical Engineering
Detroit, MI 48202

ABSTRACT
The influence of friction due to beam sliding at its supports on its dynamic behavior and its efficacy as a nonlinear isolator is studied numerically under sinusoidal and random excitation excitations. Under sinusoidal excitation, the equation of motion of the system is solved numerically and the solution is utilized to estimate the system transmissibility. It is found that when the excitation frequency is increased beyond resonance, the friction at the sliding supports serves to improve the transmissibility. The dependence of the response on initial conditions establishes the basins of attraction for different values of friction coefficient and excitation frequency and amplitude. Under random excitation, the system response statistics are estimated from Monte Carlo simulation results for different values of friction coefficient and excitation power spectral density level. The friction is found to result in a significant reduction of the system response mean square.

INTRODUCTION
Linear vibration isolators are limited for such applications of moderate environmental disturbances. However, under severe environmental disturbances such as shocks, impact loading, or ground random motion, their spectrum will definitely contain dangerous low frequencies components. The influence of isolator nonlinearity on its transmissibility depends on whether its stiffness is hard or soft [1]. It is known that soft nonlinearity causes a reduction in the resonant frequency and the isolation may be improved.

Nonlinearity becomes important in the study of an isolator when large deflections occur due to the effects of equipment weight and sustained acceleration [2]. Many researchers have conducted studies considering various combinations of restoring force and damping functions. Den Hartog [3] reported the exact solution for the vibratory response of a symmetric system with both coulomb and viscous damping when subjected to a harmonic forcing function. Ruzicka and Derby [4] presented extensive results for isolation systems with linear stiffness and nonlinear *n*-th power damping. Hundal and Parnes

[5] considered the same system when subjected to base excitation.

One of the basic requirements of vibration isolators is to reduce the system restoring force which results in a reduction of the resonant frequency. Many techniques have been developed to reduce the isolator resonant frequency. These include the curved cantilever springs for gravitational wave applications [6,7] and the triangular pre-bent cantilever springs [8-12].

The so-called "Euler spring column" has been utilized as a vertical isolator. A major advantage of the Euler spring is that it stores negligible static energy below its working range thereby minimizing both the stored elastic energy density and the spring mass required to support the suspended test mass [13,14]. The buckled or pre-bent column with fixed ends was used as a vibration isolator and analyzed by Virgin and Davis [15] and Plaut et al. [16]. It was found that for sufficiently low damping and sufficiently high column stiffness, the axial transmissibility curves exhibit an infinite number of peaks. Plaut et al. [17] considered another system consisting of two bars hinged together through a rotational spring and a rotational dashpot with one end subjected to axial excitation.

In addition to the above described isolators, other types of nonlinear isolators have been assessed by Ibrahim [18] in an extensive review article. One of the most interesting systems includes what is referred to as Gospodnetic-Frisch-Fay beam mounted on three symmetrical frictionless knife-edged supports. The beam can model a load carrying bearing for pressure pipelines against earthquake ground motion [19, 20]. The present paper is an extension of our previous work [21] which ignored the friction at the supports due to sliding. The influence of friction on the system effectiveness as a nonlinear isolator will be studied under deterministic and random excitations.

ANALYTICAL MODELING
The flexible beam considered in Somnay et al. [21] is free to slide at two knife-edged supports under the action of the load

1

Copyright © 2007 by ASME

P as shown in Figure 1(a). As the load increases both the beam length, L, and the end slope angle, ψ_0, increase as well. d denotes the displacement at the mid-span, $x = l/2$, where l is the distance between the two supports A and B. Note that L and l are only equal when the beam is horizontal without any sag. The beam deflection as a function of the applied load was originally derived by Gospodnetic [22] and Frisch-Fay [23]. For frictionless supports, the load-deflection of the beam was written in terms of the slope angle ψ as

$$\frac{Pl^2}{EI} = 8\cos\psi_o \left(\sqrt{2}\cos\psi_o \cos\phi_o + \sin\psi_o \Phi(1/\sqrt{2},\phi_o) \right)^2 \quad (1)$$

$$\frac{d}{l} = \frac{1}{2} \frac{\sqrt{2}\sin\psi_o \cos\phi_o - \cos\psi_o \Phi(1/\sqrt{2},\phi_o)}{\sqrt{2}\cos\psi_o \cos\phi_o + \sin\psi_o \Phi(1/\sqrt{2},\phi_o)} \quad (2)$$

(a)

(b)
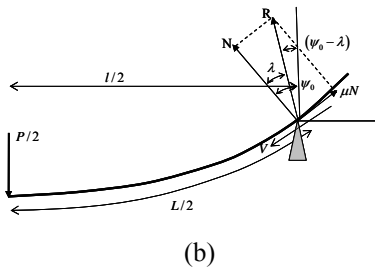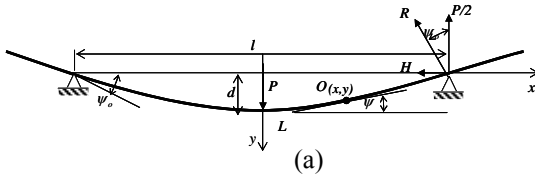
Fig. 1. Schematic diagram a flexible beam free to slide on (a) frictionless and (b) friction supports

where

$\Phi(\phi_o) = F(1/\sqrt{2},\phi_o) - K(1/\sqrt{2}) + 2E(1/\sqrt{2}) - 2E(1/\sqrt{2},\phi_o)$.

$F(1/\sqrt{2},\phi_o)$, $E(1/\sqrt{2},\phi_o)$, $K(1/\sqrt{2})$ and $E(1/\sqrt{2})$ are the incomplete integral of the first kind, the incomplete integral of the second kind, the complete integral of the first kind and the complete integral of the second kind, respectively.

If friction at the supports is considered, the reaction at the supports consists of normal and tangential components as shown in Figure 1(b). The support reaction R is inclined at an angle $(\psi_o - \lambda)$ to the vertical, where $\mu = \tan\lambda = F_f/N$, is the coefficient of friction. The vertical component of the reaction R must balance $P/2$, hence

$$R = P / \left[2\cos(\psi_o - \lambda) \right] \quad (3)$$

The equations developed in the frictionless model can be used again by replacing the term ψ_o by term $(\psi_o - \lambda)$. These equations with the appropriate substitution are:

$$\frac{Pl^2}{EI} = 8\cos(\psi_o - \lambda)\left(\sqrt{2}\cos(\psi_o - \lambda)\cos\phi_o + \sin(\psi_o - \lambda)\Phi(p,\phi_o) \right) \quad (4)$$

$$\frac{d}{l} = \frac{1}{2}\left(\frac{\sqrt{2}\sin(\psi_o - \lambda)\cos\phi_o - \cos(\psi_o - \lambda)\Phi(p,\phi_o)}{\sqrt{2}\cos(\psi_o - \lambda)\cos\phi_o + \sin(\psi_o - \lambda)\Phi(p,\phi_o)} \right) \quad (5)$$

The force-deflection relationship is approximated as best fit polynomial of the form:

$$\frac{Pl^2}{EI} = \sum_{i=0}^{5} a_{2i+1}\left(\frac{d}{l} \right)^{2n+1} \quad (6)$$

where the coefficients a_1 through a_{11} are the coefficients of the best fit polynomial.

Figure 2 shows that the friction at the support increases the critical load and deflection at which the beam becomes unstable.
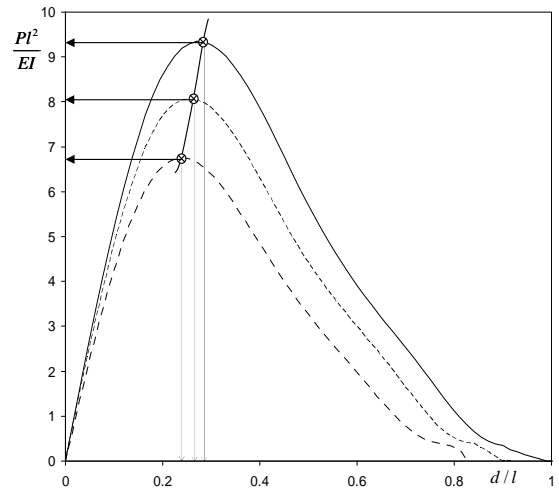
Fig. 2. Load deflection curve showing increase in critical stable load due to friction $\otimes$.
… frictionless supports $\mu = 0.0$; ------ $\mu = 0.1$; ____ $\mu = 0.2$.

The sliding velocity, V, defines the direction of the friction force. The friction-velocity relationship may be modeled as a continuous transcendental function:

$$\mu\,\mathrm{sgn}(V) \cong [\mu_k + (\mu_s - \mu_k)/\cosh(\beta V)]\tanh(\alpha V) \quad (7)$$

2   Copyright © 2007 by ASME

where μ_s and μ_k are the static and kinetic friction coefficients. α and β are parameters governing the friction curve slope at zero sliding.

Equation (7) requires a kinematical relationship between the relative sliding velocity at the support and the velocity at the beam center. The sliding velocity is given by the time derivative of the total length of the beam L, which is changing as the beam undergoes deflection. The total length is given by:

$$L = \frac{\sqrt{\cos \psi_o}}{k}\left[K(1/\sqrt{2}) - F(1/\sqrt{2}, \phi_o) \right] \quad (8)$$

The length of the sliding beam is a function of the end slope angle ψ_o, which in turn is a function of the beam center deflection, d as given by equations (5) and (6). Thus equation (8) relates the beam sliding length L to the center deflection. For our purpose it is convenient to express the relationship as a polynomial function which is obtained by curve fitting. The best fit polynomial function is expressed as:

$$L/l = 1 + l_1 \left(d/l \right)^2 \quad (9)$$

The constant $l_1 = 2.2092$. The sliding velocity at the support can be obtained by differentiating equation (9) and replacing the deflection as a non-dimensional variable to get:

$$\overline{V} = \frac{1}{2}\dot{\tilde{L}} = l_1 \tilde{d} \dot{\tilde{d}} \quad (10)$$

The end slope angle, ψ_o is expressed as a function of center displacement and the curve fit approximation of this relationship is:

$$\psi_0 = s_1 \frac{d}{l} = s_1 \tilde{d} \quad (11)$$

The constant $s_1 = 2.757$ when the end slope angle is expressed in radians. To simplify the dynamic modeling the mass of beam is neglected and the static load is only due to the weight of the carried machine of mass, m, that produces sinusoidal dynamic unbalance force, $F(t) = F_0 \sin \Omega t$, where F_0 and Ω are the excitation amplitude and frequency, respectively. The total potential energy, PE, is the sum of gravitational potential energy and elastic potential energy

$$PE = \frac{EId^2}{l^3} \sum_{i=1}^{6} \frac{a_{2i-1}}{2i}\left(\frac{d}{l} \right)^{2i-2} - mgd \quad (12)$$

The kinetic energy of the system is given by:

$$KE = \frac{1}{2}m\dot{d}^2 \quad (13)$$

The externally applied excitation force and the vertical component of the friction force are

$$Q_k = F_o \sin \Omega t + mg - \frac{\mu \, \mathrm{sgn}(\overline{V})\left(F(t) + mg \right) \cos \lambda \sin \psi_o}{\cos(\psi_o - \lambda)} \quad (14)$$

The function $\mathrm{sgn}(\overline{V})$ is used to specify the sign for the friction force as being opposed to the sliding velocity $\overline{V}$. For brevity, we introduce the friction function $F_f(\psi_o, \lambda)$ as:

$$F_f(\psi_0, \lambda) = \frac{\mu \, \mathrm{sgn}(\overline{V}) \cos \lambda \sin \psi_0}{\cos(\psi_0 - \lambda)} \quad (15)$$

Substituting equations (12) - (14) into Lagrange's equation gives the equation of motion for the isolator as:

$$m\ddot{d} + \sum_{i=1}^{6} \frac{EI \, a_{2i-1}}{l^{2i+1}} d^{2i-1} = \left[\left(F_o \sin \Omega t + mg \right)\left(1 - F_f(\psi_o, \lambda) \right) \right] \quad (16)$$

For the development of the dynamic equation of motion it is necessary to modify equation (16) such that the response displacement is measured from the static equilibrium position. This is done by defining the vibratory or perturbation component of the deflection as $y = d - S$, where S, is the static deflection and d is the total deflection. The static component is obtained from the static equilibrium equation:

$$\sum_{i=1}^{} \frac{a_{2i-1}}{l^{2i-2}} S^{2i-1} = mg\, \frac{l^3}{EI}\left(1 - \frac{\mu \cos \lambda \sin \psi_o}{\cos(\psi_o - \lambda)} \right) \quad (17)$$

Substituting for $y = d - S$, and equation (17) into equation (16) gives the equation of motion in terms of the dynamic displacement, y. Introducing the non-dimensional variables $\tilde{y} = y/l$, $\tilde{S} = S/l$, $\tau = \omega_n t$, $f_o = F_0/(ml\omega_n^2)$, $v = \Omega/\omega_n$, and adding viscous damping, equation (16) takes the form:

$$\ddot{\tilde{y}} + 2\zeta \, \dot{\tilde{y}} + \tilde{y} + \sum_{i=1}^{10} c_{i+1} \tilde{y}^{i+1} = f_o \sin v\tau \left\{ 1 - F_f\left(\psi_o \lambda \right) \right\} \quad (18)$$

where ω_n is the linear natural frequency of the beam, and other coefficients are constants.

Substituting the kinematical relationships for $\overline{V}$ and ψ_o as given by equations (10) and (11) into the expression for F_f

3

Copyright © 2007 by ASME

equation (16) allows us to express F_f as a function of the central deflection d as:

$$F_f(\psi_0, \overline{V}, \lambda) = F_f\left(d, \overline{V}, \lambda\right) = \frac{\mu \, \text{sgn}(\overline{V}) \cos \lambda \sin(s_1 d)}{\cos\left[(s_1 d) - \lambda\right]} \quad (19)$$

The equation of motion (19) will be numerically solved to evaluate the steady state response to a harmonic excitation.

STEADY STATE RESPONSE

The dependence of the friction force on the velocity in the vicinity of zero sliding velocity is characterized by a steep gradient. This feature makes the equation of motion belongs to a 'stiff' system in the numerical integration. Beginning with prescribed initial conditions, the Solver steps through the time interval, computes a solution at each time step using a user supplied subroutine which evaluates the force function together with its derivative. The solution for a given time step is converged if it satisfies the user specified error tolerance criteria, taken as 10^{-6}.

The equation of motion for the frictional isolator (18) is reproduced here after dropping the over-tilde notation and transposing the frictional force term F_f to the left hand side:

$$\ddot{y} + 2\zeta \dot{y} + F_f\left(\psi_o, \overline{V}, \lambda\right) f_o \sin \nu\tau + y + \sum_{i=1}^{10} c_{i+1} \tilde{y}^{i+1} = f_o \sin \nu\tau \quad (20)$$

Here $F_f\left(\psi_o, \overline{V}, \lambda\right)$ is the friction force at the support along the direction of motion, and is given by equation (19)

$$F_f(\psi_0, \overline{V}, \lambda) = \frac{\mu \, \text{sgn}(\overline{V}) \cos \lambda \sin \psi_0}{\cos(\psi_0 - \lambda)} \quad (21)$$

where λ is the friction angle. The expression for the total transmitted force F_t at the support is:

$$F_t = \sqrt{F_{te}^2 + (F_{td} + F_{tf})^2} \quad (22)$$

where F_{te}, F_{td} and F_{tf} are the transmitted elastic, damping and friction forces, respectively. Using the absolute magnitudes of the terms in equation (21) the friction force component F_{tf} will be:

$$F_{tf} = \frac{f_o \mu \cos \lambda \sin(s_1 a)}{\cos(s_1 a - \lambda)} \quad (23)$$

Here a is the displacement amplitude obtained from the numerical simulation and $s_1 = 2.757$ is the curve fit coefficient of the end slope deflection equation. Incorporating equations (22) and (23) into the definition of the transmissibility gives:

$$TR_{fr} = \frac{F_t}{f_o} \quad (24)$$

Figure 3 shows the effect of the sliding friction on the transmissibility of linear and nonlinear isolators for $\mu_s = 0.5$ and $\mu_k = 0.3$. It is seen that the transmissibility of the frictional isolator in the low frequency regime is improved when compared with the frictionless isolator and is superior to the linear one. When the excitation frequency is increased beyond resonance, the friction at the sliding support serves to improve the transmissibility when compared with the linear isolator. This improvement is attributed to the reduction in the amplitude of vibration that is a result of the opposing friction force.
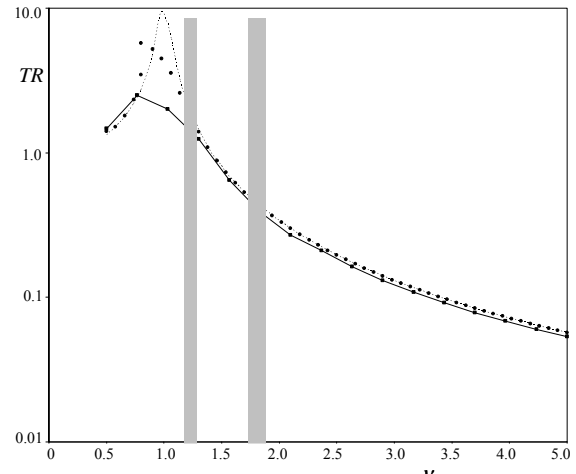
Fig. 3. Comparison of the transmissibility of - - - : Linear isolator; ••• : Non linear isolator without friction; ▪▪▪▪ Non-linear isolator with friction.
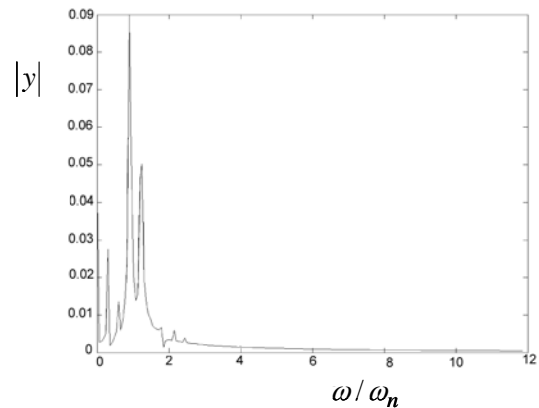
Fig. 4. FFT plot showing response frequency components at excitation frequency $\nu = 1.22$. and $f_o = 0.025$, $\mu_s = 0.5$ and $\mu_k = 0.3$,.

4   Copyright © 2007 by ASME

The friction also introduces regimes where there is multi-periodic response. These are indicated by the shaded grey regions in Fig. 3. The response frequency components over a time window of 50 units are shown in the *FFT* plot in Fig. 4. It is seen that due the asymmetry about the time axis, the response possesses non-zero mean, which is reflected in the FFT at zero frequency. The side frequencies that appear the excitation frequency ratio ν =1.22 are attributed to the inherent nonlinearity of the isolator. Under excitation frequency ratio ν =1.94, the response dynamic characteristics are shifted to mono-periodic non-harmonic oscillations. Under an increased excitation amplitude of f_o =0.04 there is the non-harmonic period doubling response at the low excitation frequency ν =0.5.

(a) $\mu_k = 0.0$

(b) $\mu_k = 0.275$
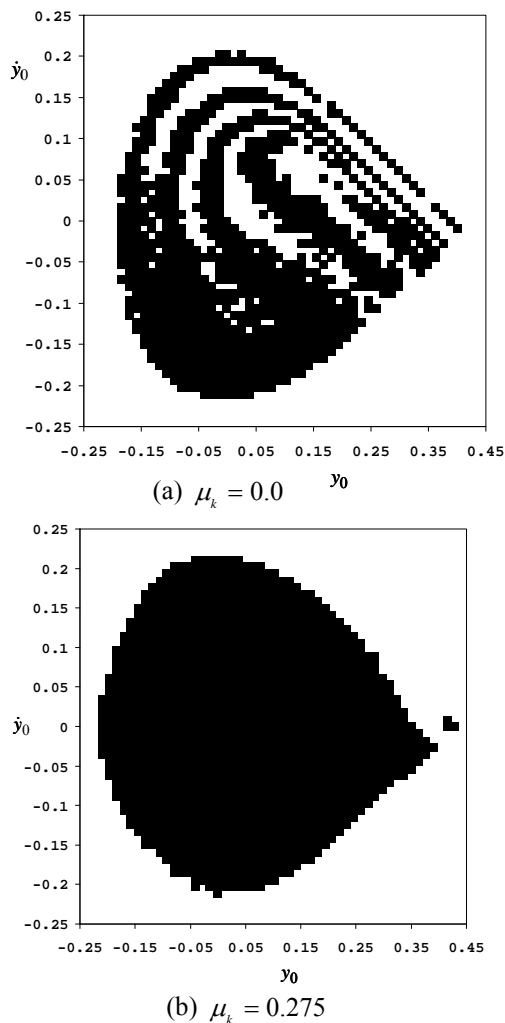
Figure 5. Safe basins of attraction showing different response characteristics for two different values of friction coefficient.

$$\nu = 0.85 \text{ and } f_o = 0.0302$$

■: Stable periodic non-harmonic response; Empty space: un-bounded

BASINS OF ATTRACTION

The dependence of the response on the initial conditions establishes the basins of attraction. Figs 5(a) and (b) show the how the basins of attraction are affected by the value of the friction coefficient. It is seen that the friction at the support restrains the beam and limits its deflection to a lower level than the point of instability. In the limiting case when the friction is infinitely large any sliding at the support will be prevented and the beam would be constrained to a fixed length. This would physically resemble a beam on simple supports which is stable for all sets of initial conditions over the entire phase plane. Throughout this study the frictional isolator response shows a strong dependence on initial conditions.
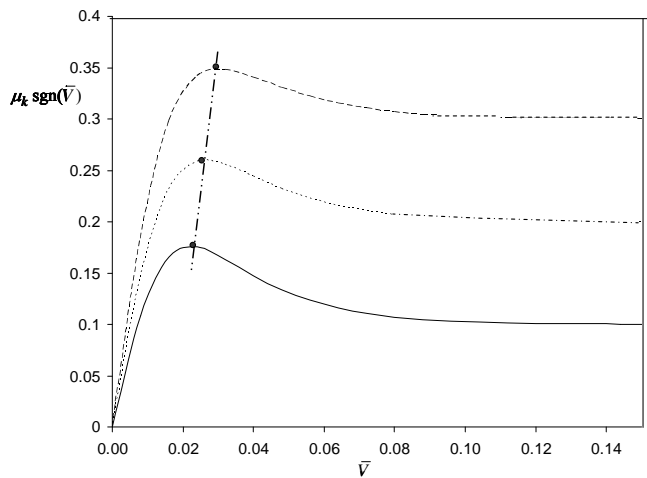
Fig. 6. Friction Coefficient vs. relative velocity for three values of kinetic friction. —— $\mu_k = 0.1$, $-\cdot-\cdot-\mu_k = 0.2$, and

$---\mu_k = 0.3$. $\cdots-\bullet-\cdots$ peak location

The numerical representation of the friction-velocity relationship (7) for three different values of kinetic friction is shown in Figure 6. The dashed-solid point curve defines the locus of the friction peak where the slope of each curve is zero and any further increase in the sliding velocity produces a negative slope. This Figure will help in better understanding the safety integrity factor. The safety integrity factor (also referred to as the stability fraction) is defined by the ratio of the area of the stable region in the phase plane (area of the safe basin) to the total area encompassed S_f by the homoclinic orbit. S_f is evaluated for different levels of excitation parameters. Figure 7 shows the dependence of the safety integrity factor on the excitation amplitude level for these three different values of friction coefficient in addition to the zero friction case (indicated by the solid curve). All three curves show the tendency of the friction to prolong the stable region as

5   Copyright © 2007 by ASME

reflected in the longer plateau where S_f stays just under 1.0. However, it is observed that beyond a critical value of force amplitude f_o, the curve drops off sharply. The points where the frictional curve intersects with the zero friction curve indicates a transition where the sliding friction at the supports is no longer beneficial in stabilizing the beam vibration. These points are marked as solid circles in Figure 6. A closer examination of the state variables at these points indicates that the velocity amplitude under the corresponding excitation force reaches the critical values identified in Figure 6 where the slope of the friction-velocity curve turns negative.
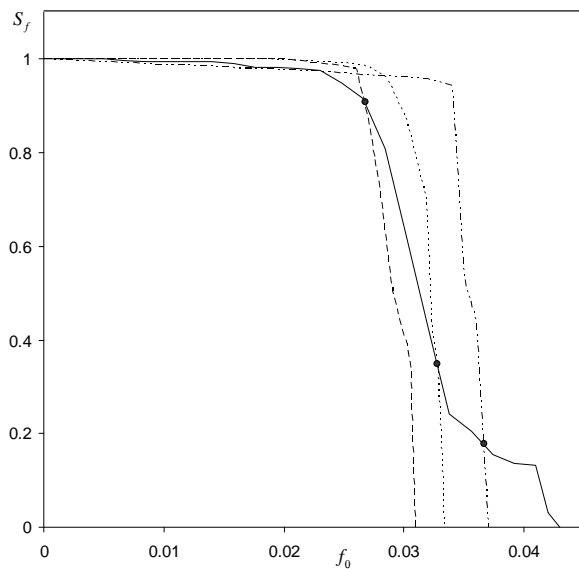
Fig. 7. Dependence of safety integrity factor on excitation amplitude level for three different values of friction coefficient.
____ $\mu_k = 0.0$; − − − $\mu_k = 0.1$; ••• $\mu_k = 0.2$; − · − · − $\mu_k = 0.3$
● : Crossing Points

RANDOM EXCITATION OF THE ISOLATOR
The equation of motion which defines the response of the flexible beam isolator subjected to a white noise excitation $W(\tau)$ takes the form:

$$\ddot{y} + 2\zeta \, \dot{y} + y + \sum_{i=1}^{10} c_{i+1} \tilde{y}^{i+1} = W(\tau)(1 - F_f(\psi_o, \lambda)) \qquad (25)$$

The power spectral density function of the input excitation is evaluated for each excitation record to verify that it is a constant value over a wide frequency band. The time integration of the equation (25) for the specific excitation record is followed by evaluating the response statistics in the time, frequency and amplitude domains. In the time domain the mean $E[y]$ and mean square $E[y^2]$ time histories are

evaluated. The Monte Carlo simulation is carried out for different values of excitation intensity levels, $\pi S_o/2\zeta$. For each excitation intensity level the response is obtained for the frictionless beam and for the beam with the support friction coefficient $\mu_k = 0.3$. Two selected samples are shown in Figs 8(a) and (b) for $\pi S_o/2\zeta = 0.006$ and 0.02366, respectively. The mean square time history approaches a stationary state at a level of 0.0045. This value is lower than the corresponding frictionless response mean square converged level which is indicated by a dashed line. This is attributed to the restraining effect that the friction has in reducing the amplitude of the response.
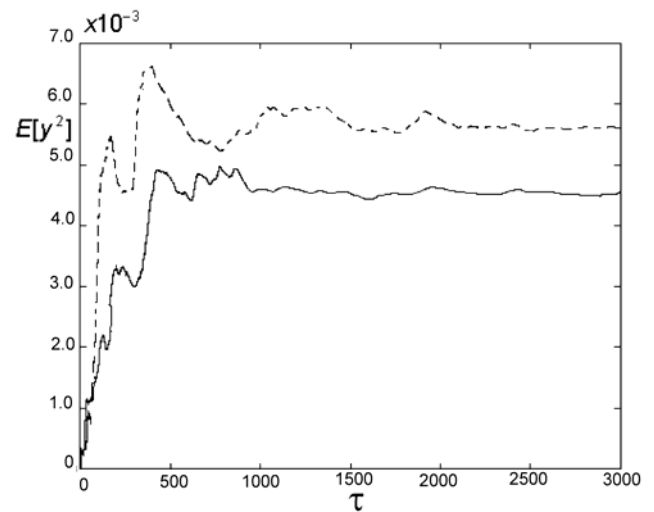
(a) $\pi S_o / 2\zeta = 0.006$, $\mu = 0.3$.
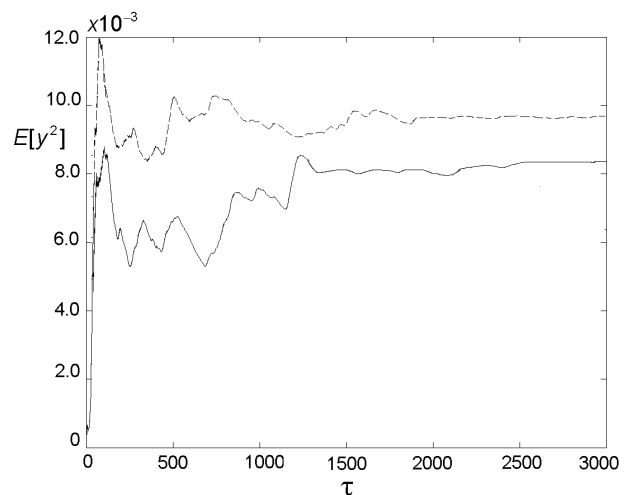
(b) $\pi S_o / 2\zeta = 0.02365$, $\mu = 0.3$.
Fig. 8 Mean square responses for two different values of excitation level in the presence (——) and absence (- - -) of friction.

6   Copyright © 2007 by ASME

The excitation intensity $\pi S_o/2\zeta = 0.02366$ is identified as the limit based on the homoclinic orbit. Fig. 8(b) shows the mean square response, which stays consistently below the frictionless system response. The Monte Carlo simulations of both the frictionless and frictional isolator show non-stationary responses for excitation levels beyond $\pi S_o/2\zeta = 0.02365$ which coincides with the maximum excitation level to maintain the homoclinic orbit of the unperturbed beam.
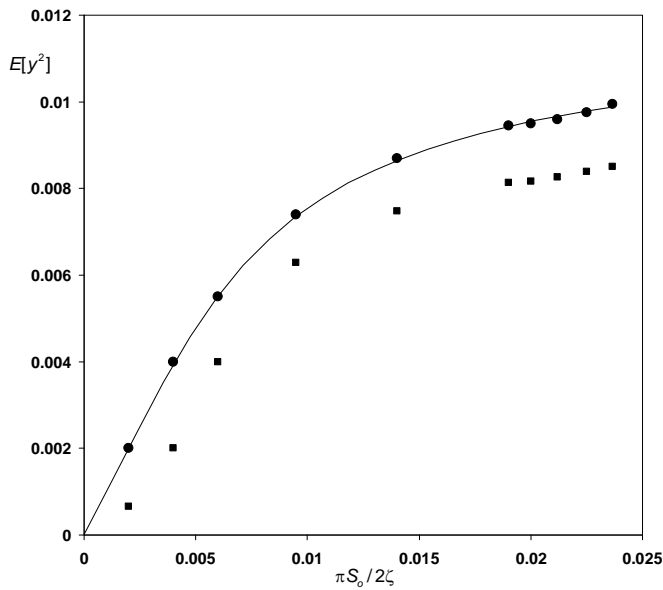
Fig. 9. Dependence of mean square response on excitation intensity level.

• • • Frictionless case

■ ■ ■ ■: with friction $\mu_s = 0.5$; $\mu_k = 0.3$

———: Analytical prediction in the absence of friction.

Figure 9 shows the results of the Monte Carlo simulation presented as the dependence of the mean square response $E[y^2]$ on the intensity of the $\pi S_o/2\zeta$. The circles on the graph represent the responses obtained for the frictionless isolator and the squares for the frictional isolator with $\mu_k = 0.3$. Also, the closed form solution for the frictionless isolator (see, Somnay, et al. 2006) is plotted in Figure 10. The converged value of the mean square, $E[y^2]$, closely matches the expected value of the total energy $E[H]$ of the closed form solution. The onset of non-linearity in the response which occurs at excitation intensity level $\pi S_o/2\zeta = 0.006$ is also indicated in both the closed form and simulation results.

VI. CONCLUSIONS

The influence of friction due to beam sliding at its ends on its dynamic behavior and its efficacy as a nonlinear isolator has been studied numerically under sinusoidal and random excitations. Under sinusoidal excitation, the equation of motion of the system is solved numerically and the solution is utilized to estimate the system transmissibility. It was found that when the excitation frequency is increased beyond resonance, the friction at the sliding supports serves to improve the transmissibility. The dependence of the safety integrity factor on excitation amplitude level and friction coefficient reveals that the friction extends the stable region. Under random excitation, the system response statistics were estimated from Monte Carlo simulation results for different values of friction coefficient and excitation power spectral density level. The friction is found to result in a significant reduction of the system response mean square.

References

 [1] Kolovsky, M. Z., 1999, *Nonlinear Dynamics of Active and Passive Systems of Vibration Protection*, Springer-Verlag, Berlin.

[2] Yuryev, G. S., 1991, *Vibration Isolation of Precision Instruments*, (in Russian) Russian Academy of Sciences, Siberian Branch, Institute of Nuclear Physics Press, Novosibirsk, Reprint 89-146.

[3] Den Hartog, J. P., 1931 "Forced vibrations with constrained coulomb damping and viscous friction," Transactions of the ASME **53**, 107-115.

[4] Ruzicka, J. E., and Derby, T. F., 1971, *Influence of Damping in Vibration Isolation*, Washington, D.C., The Shock and Vibration Information Center.

[5] Hundal, M. S. Parnes, P. S., 1979, "Response of a base excitation system with Coulomb and viscous friction," *Journal of Sound and Vibration* **64**, 371-378.

[6] Blair, D. G., van Kann, F. J., and Fairhall, A.L., 1991, "Behavior of a vibration isolator suitable for use in cryogenic or vacuum environments," *Measurement Science and Technology* **2**, 846-850.

[7] Ju, L. and Blair, D. G., 1994,"Low resonant frequency cantilever spring isolator for gravitational wave detectors," *Review of Scientific Instruments* **65**(11), 3482-3488.

[8] Losurdo, G., Bernardini, M., Braccini, et al., 1999, "An inverted pendulum pre-isolator stage for the VIRGO suspension system," *Review of Scientific Instruments* **70**(5), 2507-2515.

[9] Plissi, M. V., Torrie, C. I., Husman, M. E., Robertson, N. A., Strain, K. A., Ward, H., Lück, H., Hough, J., 2000, "GEO 600 triple pendulum suspension system: Seismic isolation and control," *Review of Scientific Instruments* **71**(6), 2539-2545.

[10] Ballardin, G., Bracci, L., Braccini, S., et al., 2001, "Measurement of the VIGRO super-attenuator performance

7   Copyright © 2007 by ASME

for seismic noise suppression," *Review of Scientific Instruments* **72**(9), 3643-3652.

[11] Takahashi, R., Kuwahara, F., Majorana, et al., 2002a, "Vacuum-compatible vibration isolation stack for an interferometric gravitational wave detector TAMA300," *Review of Scientific Instrument* **73**(6), 2428-2433.

[12] Takahashi, R, Arai, K., and the TAMA Collaboration, 200b, "Improvement of the vibration isolation system for TAMA300," *Classical and Quantum Gravity* **19**, 1599-1604.

[13] Winterflood, J., Blair, D. G., and Slagmolen, B., 2002a, "High performance vibration isolation using springs in Euler column buckling mode," *Physics Letters A* **300**, 122-130.

[14] Winterflood, J., Barber, T. A., and Blair, D. G., 2002b, "Mathematical analysis of an Euler spring vibration isolator," *Physics Letters A* **300**, 131-139.

[15] Virgin, L. N. and Davis, R. B., 2003, "Vibration isolation using buckled structures," *Journal of Sound and Structures* **260**, 965-973.

[16] Plaut, R. H., Sidbury, J. E., and Virgin, L. N., 2005a, "Analysis of buckled and pre-bent fixed-end columns used as vibration isolators," *Journal of Sound and Vibration* **283**, 1216-1228.

[17] Plaut, R. H., Alloway, L. A., and Virgin, L. N., 2005b, "Nonlinear oscillations of a buckled mechanism used as a vibration isolator," Proceedings of the IUTAM Symposium on *Chaotic Dynamics and Control of Systems and Processes in Mechanics*, G. Rega and F. Vestroni (Eds.), Springer, The Netherlands, 241-250.

[18] Ibrahim, R. A., 2007, "Recent advances in nonlinear vibration isolators," Submitted for possible publication in Journal of Sound and Vibration.

[19] Kisliakov, D., 1999a, "Dynamic analysis of a multiple-supported pressure pipeline subjected to both axial and vertical seismic excitation components," Proceedings of the 3rd International Conference on Seismology and Earthquake Engineering, Iran, II:881-898.

[20] Kisliakov, D., 1999b, "Axial earthquake-induced vibrations of a pressure pipeline on frictional support columns," Proceedings of the Anniversary Scientific Conference on 50 years Faculty of Hydraulic Engineering at UACEG, Sofia, Vol. III.

[21] Somnay, R., Ibrahim, R. A., and Banasik, R. C., 2006, "Nonlinear Dynamics of a Sliding Beam on Two Supports and Its Efficacy as a Non-Traditional Isolator," *Journal of Vibration and Control* **12**(7), 685-712.

[22] Gospodnetic, D., 1959, "Deflection curve of a simply supported beam," A*SME Journal of Applied Mechanics* **26**, 675-676.

[23] Frisch-Fay, R., 1962, *Flexible Bars*, Butterworths, London.